buildings

Article

Numerical Study on the Dynamic Behaviors of Masonry Wall under Far-Range Explosions

Yi Zhang [1], Jiahui Hu [2,*], Wenda Zhao [3,*], Feng Hu [1] and Xiao Yu [1]

1 Institute of Defense Engineering, AMS, PLA, Beijing 100850, China
2 College of Civil Engineering, Tongji University, Shanghai 200092, China
3 China Construction Engineering Bureau Co., Ltd., Shanghai 200122, China
* Correspondence: hujiahui@tongji.edu.cn (J.H.); zhaowenda@cscec.com (W.Z.)

Abstract: As a common enclosure structure, masonry walls are widely used in various types of buildings. However, due to the weak out-of-plane resistance of masonry walls and the generally brittle properties of the materials used for blocks, they are highly susceptible to collapse under blast loads and produce high-speed splash fragments, which seriously threatens the safety of personnel and equipment inside buildings. In this paper, based on the existing tests, a refined numerical simulation model was established to carry out numerical studies of clay tile walls and grouted CMU masonry infill walls under far-range blast loads, and the applicability of the finite element model and parameters were verified. Further, the effects of wall boundary configuration, constraints and dimensions on the dynamic response of the walls were carried out. The results show that: the load distribution on the wall is relatively uniform under the far-range explosion and can be considered as uniform load; the blast-resistant performance of the wall can be enhanced by increasing the grouting rate and the uniformity of grout hole distribution; the boundary configuration of the wall has little effect on the blast resistance, while the boundary constraints and the length and width are the main factors affecting the blast resistance of the wall.

Keywords: far-range explosion; numerical simulation; masonry walls; dynamic response; damage

Citation: Zhang, Y.; Hu, J.; Zhao, W.; Hu, F.; Yu, X. Numerical Study on the Dynamic Behaviors of Masonry Wall under Far-Range Explosions. *Buildings* **2023**, *13*, 443. https://doi.org/10.3390/buildings13020443

Academic Editor: Elena Ferretti

Received: 14 November 2022
Revised: 11 December 2022
Accepted: 15 December 2022
Published: 6 February 2023

1. Introduction

Masonry walls are widely used around the world due to their excellent performance, low cost, and easy accessibility. Ettouney et al. [1] estimated that more than 70% of the world's existing buildings are masonry structures, in addition the majority of building envelopes are dominated by the masonry infill wall (MIW). American blast consultants ABS [2] found that up to 75% of the casualties in terrorist attacks come from the secondary injuries caused by flying debris from windows, doors, glass and walls in explosions. Therefore, it is of significant value to study the blast resistance of masonry walls.

The explosion load mainly depends on the scaled standoff distance $Z = R/W^{1/3}$, where R is the distance between the charge and the structure, W is the charge of TNT equivalent. The impact of blast loads on structures differs greatly with different scaled standoff distance Z, and Orton [3] summarized relevant research on the structural response under blast loads and divided the blast scenarios according to Z: for the wall-slab members, it subjected to near-range explosion when $Z \leq 0.4$ m/kg$^{1/3}$, medium-range when $0.4 \leq Z \leq 1.0$ m/kg$^{1/3}$, and far-range when $Z > 1.0$ m/kg$^{1/3}$. At present, the far-range field explosion specified by ASCE, (scaled distance $Z > 1.2$ m/kg$^{1/3}$), is adopted to ensure the uniformly distributed blast overpressure acted on the target wall.

As for the study of the blast resistant performance of masonry walls, Varma et al. [4] carried out a blast test study on 27 pieces of 3 m × 3 m common clay brick walls under a variety of blast load conditions mainly at $2.2 \leq Z \leq 4.4$ m/kg$^{1/3}$ and $1.0 \leq Z \leq 2.0$ m/kg$^{1/3}$, and obtained the dependence of the damage level of the wall on the blast impulse with the influence of wall thickness and wall boundary configuration.

Davidson et al. [5] investigated the blast resistance of 9 differently configurated unidirectional restrained walls with hollow concrete masonry units (CMU), including 6-inch-thick partially grouted CMU walls, 8-inch-thick partially grouted CMU walls, and 8-inch-thick partially grouted CMU walls with clay finish brick facings, by blast tests at different scaled distances. The study showed that the ductility of the CMU walls is significantly improved after grouting and reinforcement; in addition, the clay brick facing outside the walls have a good energy absorption effect, which could reduce the deformation and displacement of the walls to a certain extent, but it usually produced damage and outwardly scattered debris in the explosion.

Fang et al. [6] investigated the blast resistance of common clay brick walls at scaled distances in the range of $1.8 \sim 10.0\ \mathrm{m/kg^{1/3}}$ by conducting 12 blast tests. The damage pattern of the wall and the fragment dispersion and distribution under the blast load were analyzed, and the development of wall cracking as well as the effects of boundary conditions and charge weight on the damage pattern and level of the wall were further explored by numerical simulations. In addition, Keys and Clubley [7] conducted an experimental study of the dynamic response and brick dispersion pattern of 10 pieces of masonry walls under uniform blast surface loads with a positive pressure duration of more than 100 ms based on a large-sectional shock tube.

Shi et al. [8] studied the damage pattern and debris splash law of common clay brick infill walls under near-range blast loads of $Z = 0.4\ \mathrm{m/kg^{1/3}}$ and $Z = 0.22\ \mathrm{m/kg^{1/3}}$ through the blast test, and further proposed a blast-resistant reinforcement system for common masonry brick walls with dry-hanging slabs. The test shows that: with blast standoff of 0.4 m and charge weight of 1 kg and 6 kg, compared to the blast resistant performance of common masonry brick walls and commercial blast panel reinforced masonry brick walls, dry-hanging stone slab reinforcement has a more excellent blast-resistant performance: the total mass of splash block fragments reduced by 71.8%, the maximum splash distance reduced by 83.3%.

Numerical simulation is an effective complement to the study in this field due to the high cost and discrete results of wall blast tests. Based on the tests of Varma et al. [5], Wei et al. [9] proposed a quantitative method for classifying wall damage based on the maximum deflection of the wall, as well as the relationship between the rotation at the support and the wall thickness. Numerical simulations were conducted to verify the work, analyzing the effects of parameters, e.g., mortar strength, block strength, boundary constraints and wall thickness. The results show that the boundary restraint conditions, and wall thickness have a significant effect on the dynamic response of walls under blast loading, while the material strength of the blocks cast smaller influence.

Hao et al. [10] further investigated the damage severity of low-rise reinforced concrete frames with infill masonry walls subjected to blast loading through numerical simulations, which classified the damage levels by scaled standoff distance: (1) when $Z \leq 1.82\ \mathrm{m/kg^{1/3}}$, the structure undergoes overall collapse; (2) when $1.82 \leq Z \leq 4.5\ \mathrm{m/kg^{1/3}}$, only the infill wall collapsed; (3) when $4.5 \leq Z \leq 5.0\ \mathrm{m/kg^{1/3}}$, the infill wall was damaged without collapse; (4) when $Z > 5.0\ \mathrm{m/kg^{1/3}}$, residual deformation appears on the front surface of the wall with no significant damage. Hao et al. [10,11] measured the dynamic properties of concrete block and mortar materials by uniaxial compression tests at different strain rates, obtained an empirical formula for the dynamic increasing factor (DIF) for block and mortar materials, and prepared an orthogonal homogenized material model that can be applied to materials such as brick, stone, and mortar considering strain rate effects.

Michaloudi and Gebbeken [12] further developed the finite element (FE) method for blast resistance simulation of common clay brick walls by introducing Riedel–Hiermaier–Thoma (RHT) model and the node-split algorithm in order to improve the effectiveness of the FE method in simulating the fragments of the wall and the local damage under contact and near-range explosions. Additionally, contact explosion and far-range explosion tests of 0.25 kg charge weight and were carried out, respectively.

In recent years, several experimental and numerical investigations on the dynamic behaviors of masonry walls have been further carried out [13–18]. Li et al. [19] conducted vented gas explosion tests on the one-way clay brick and autoclaved aerated concrete (AAC) MIW, indicating that the response mode of MIW under gas explosion loads is similar to that under quasi-static loadings attributed to the relatively long blast pressure duration. Türkmen et al. [20] utilized six point-bending test setup to examine the out-of-plane quasi-dynamic cyclic behaviors of one-way masonry wall with loading rates of 30 mm/s. It showed that the out-of-plane load-bearing capacity was nearly linearly decaying after the peak load, and the maximum central deflection could reach the thickness of wall. In addition, the numerical simulation methods, e.g., finite element, discrete element, smoothed particle hydrodynamics, etc., have been developed to conduct more comprehensive studies as a supplement to the experiment. Mollaei et al. [21] conducted FE simulation of one-way AAC masonry wall to investigate the blast resistance with different thicknesses, indicating that the wall constructed with AAC blocks have poor anti-blast performance. Michaloudis and Gebbeken [12] adopted the simplified separated model to conduct FE analyses of masonry wall under the far-range and contact explosion loadings, and a node-split modeling approach was employed in the masonry elements to accurately capture the local damage of walls subjected to contact explosive loading.

However, most of the above research focus on unidirectional masonry walls with unidirectional boundary constraints, i.e., the upper and lower boundary of the masonry wall is connected with the frame, while the left and right sides are separated from the frame. Though such one-way masonry wall is rarely used in construction practice, instead, the two-way walls is more commonly used, and correspondingly is the main research object of this paper.

In this paper, based on the far-range blast tests conducted by Varma et al. [4] and Davidson et al. [5], commercial FE analysis software LS-DYNA [22] was used to establish the FE models of solid clay brick walls and CMU masonry walls under far-range blast loads, and the results were compared with the test data for verification. The effects of blast distance, bonding strength at block-mortar interface and constitutive model of block material under near-range explosion were further discussed.

2. Finite Element Modeling

FE models for masonry walls are mainly divided into two types: homogenized and separated. The homogenized model is more computationally efficient, but it cannot accurately describe the basic characteristics of masonry, e.g., cracking damage along the mortar layer. In the separated model the masonry and mortar are modeled separately, and the mutual interaction is simulated by setting up contact. Although it is more computationally intensive, it can better reflect the difference in mechanical properties of blocks and mortar and simulate the bond slip and damage that occurs in the structurally weak layer formed by the block-mortar bonding interface. In this paper, based on FE software LS-DYNA, the 8-node hexahedral solid units were utilized to establish the separated refinement model of the wall, as shown in Figure 1.

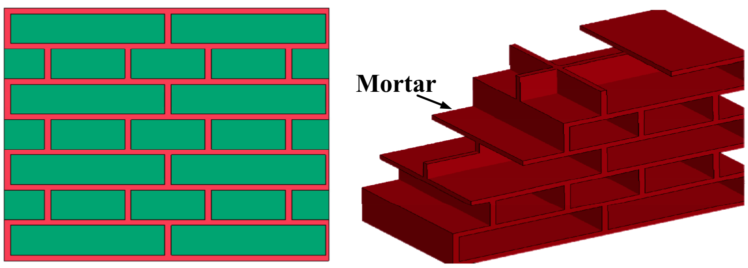

Figure 1. Separated model of masonry wall.

2.1. Interface Contact and Parameters

Since actual masonry structures are bonded by mortar between both the blocks and mortar, as well as the walls and concrete frames, the keyword * Automatic_Contact_Surface_To_Surface_Tiebreak is used in this paper to describe the criteria for determining contact failure as Equation (1) [22]. When the ultimate tensile stress or shear stress is reached, the interface is bound together. When the limit value is exceeded, the interface breaks, and the contact will degenerate into automatic surface-to-surface contact, which can only bear the pressure of re-contact, but cannot transfer the tension and shear.

$$\left(\frac{f_n}{F_n}\right)^2 + \left(\frac{f_s}{F_s}\right)^2 > 1 \tag{1}$$

where f_n is the actual positive stress in the bond interface, f_s is the actual shear stress on the bond interface, F_n and F_s are the allowable positive and shear stresses on the contact surface, i.e., the tensile and shear strength of the masonry, respectively. The use of Tiebreak type contact can better reflect the slip and shear-tension damage between masonry blocks and mortar in the wall.

Following design code GB50003 [23], the calculation formulas for the average tensile strength $f_{tm,\ m}$ and shear strength $f_{v,\ m}$ of masonry bending along through joints are shown in Equation (2) and Equation (3), respectively, where f_2 is the average compressive strength of mortar.

$$f_{tm,m} = 0.125\sqrt{f_2} \tag{2}$$

$$f_{v,m} = 0.125\sqrt{f_2} \tag{3}$$

As the wall model is prone to large deformation under blast load in FE simulation, the mesh tends to undergo distortion. In order to prevent this phenomenon and at the same time to better simulate the damage occurring in the wall under the blast load, the * MAT_ADD_EROSION keyword is added to the mortar model considering that the damage occurs mainly along the mortar layer in the test, and the main strain term MXEPS is adopted as the cell deletion criterion. However, the unit deletion algorithm and the value of failure strain lack the relevant physical basis and theoretical basis, and too much deletion leads to the non-conservation of structural energy and mass, making the results deviated. Thus, the value is mainly based on the trial calculation results and determined as 0.005.

2.2. Material Models and Parameters

Solid clay bricks and mortar are a type of brittle material of concrete, and the BRITTLE DAMAGE model No. MAT_96 is used. When using this material model, the tensile and shear strengths in the material degrade with the development of cracks caused by tensile stresses, thus simulating the accumulation of damage in the material. The main input parameters of this model are density, modulus of elasticity, compressive strength, tensile strength, shear strength, etc. In Refs. [24,25], empirical formulas for the elastic modulus of blocks E_b and the elastic modulus of mortar E_m were fitted based on a large amount of experimental data, as shown in Equation (4) and Equation (5), respectively. Where f_1 is the average compressive strength of block and f_2 is the average compressive strength of mortar.

$$E_b = 4467 f_1^{0.22} \tag{4}$$

$$E_m = 1057 f_2^{0.84} \tag{5}$$

Based on the mechanical properties of the clay bricks in the Varma test, the compressive strengths of the blocks and mortar are taken as 12.24 MPa and 5.0 MPa, respectively, and the elastic modulus of the blocks E_b and the elastic modulus of the mortar E_m are still calculated according to Equations (4) and (5), as shown in Table 1.

Table 1. Parameters of clay block and mortar material model.

Material	Density (kg/m³)	Young's Modulus (MPa)	Poisson's Ratio	Ultimate Compression Strength (MPa)	Ultimate Shear Strength (MPa)	Fracture Toughness (N/m)	Shear Retention Rate	Bulk Viscosity (MPa/s)	Compression Strength (MPa)
Clay brick	1800	8163	0.16	1.94	3.5	140	0.03	0.72	12.24
Mortar	1800	4016	0.21	0.55	0.95	140	0.03	0.72	4.9

As for the hollow CMU blocks, it has been shown that the Soil and Foam model of MAT_5 can better characterize their mechanical properties under blast loading [26] with the parameters shown in the following table. In order to better simulate the damage pattern of the wall under explosion loading and prevent element distortion, * MAT_ADD_EROSION is added to the mortar model, and through trial and error, it is determined that the result is optimal when the maximum principal strain MXEPS of the element is taken as the failure criterion, and the value is 0.005. The corresponding parameters and their values are listed in Table 2.

Table 2. CMU block material model parameters.

Density (kg/m³)	Shear Modulus (MPa)	Bulk Modulus (MPa)	A_0	A_1	A_2	Tensile Strength (MPa)
1900	5433	41,368	0.616	0	0	1.38

Since the dynamic response and damage pattern of the wall are mainly considered in this simulation, and the damage of the external frame of the wall in the test is relatively minor in general, based on the consideration of computational efficiency, the MAT_RIGID model is used and its rotation and displacement in any direction are restricted.

3. Model Validation

3.1. Explosion Test of Clay Brick Wall

It should be noted that, because the experimental research in this field in the United States is relatively adequate, the discussion in this paper mostly adopted American experiments to verify the model and modeling method. The model based on verification can further carry out numerical analysis on walls of construction practice in various countries.

Varma et al. [4] conducted a systematic test on the blast resistance of common sintered brick MIWs, and 27 pieces of 3 m × 3 m common clay brick walls were blast tested in total. The effects of three different wall boundary configurations of common boundary, reinforced boundary and slotted boundary were studied, and the effects of three different wall thicknesses of 230 mm, 350 mm and 460 mm were focused on, with block sizes of 230 mm × 115 mm × 75 mm. Figure 2 gives the wall dimensions, the three different forms of wall boundary configurations, and the FE model established in this paper is shown in Figure 3.

According to the different scaled standoff distances, the test was conducted in two categories ($2.2 \leq Z \leq 4.4\ \mathrm{m/kg^{1/3}}$ and $1.0 \leq Z \leq 2.0\ \mathrm{m/kg^{1/3}}$), and the charge shapes were mainly spherical or hemispherical TNT or Topex II explosives. The data measured in the test includes the maximum deflection at the center of the wall, peak reflection overpressure and reflection impulse. In the test category with larger scaled standoff ($2.2 \leq Z \leq 4.4\ \mathrm{m/kg^{1/3}}$), the wall response was mainly in the elastic phase and no significant damage occurred; as the scaled standoff decreased ($1.0 \leq Z \leq 2.0\ \mathrm{m/kg^{1/3}}$), the wall deformation and the accumulated damage increased significantly. By evaluating and grading the damage level of the wall in the test, the wall damage can be classified from high to low as A (complete collapse), B (large cracking and bending of the wall beyond repair), C (striking cracks between the extended bricks or between the brick and frame joints, and cracks also appear in the brick body), and D (minor damage to the surface layer).

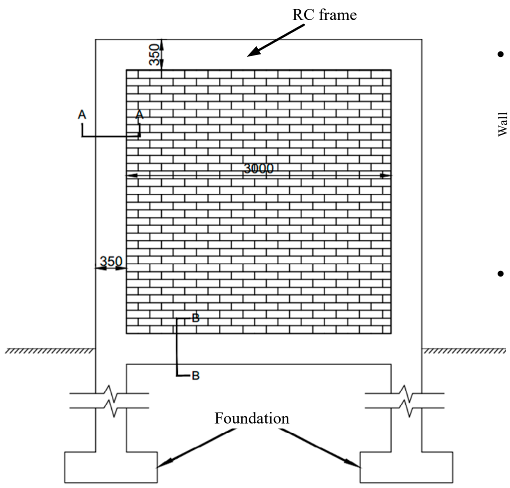

Figure 2. Diagram of test setups.

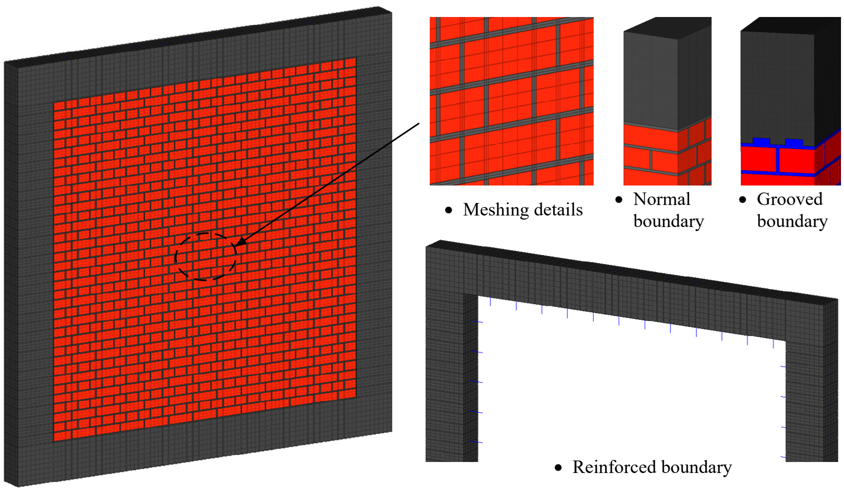

Figure 3. FE model of clay brick MIW.

Block and mortar are quasi-concrete brittle materials, therefore, MAT _ 96 BRITTLE DAMAGE model was adopted for Varma's test. When this material model is utilized, the tensile and shear strength of the material will degrade with the development of cracks caused by tensile stress, thus the damage accumulation in the material is simulated.

In order to ensure the calculation efficiency, the mortar layer is divided into only one layer of grid in the thickness direction, and the mesh size is in accordance with the brick in the other two directions. The mesh sensitivity analysis is carried out for bricks with mesh sizes of 20 mm, 30 mm and 40 mm on the dynamic response of 230 mm thick wall under the blast scenario with 3.3 kg charge weight and 5 m standoff. The displacement-time histories of the wall center with different mesh sizes and the corresponding peak deflections are shown in Figure 4. It can be seen that with the decrease in the mesh size, the overall stiffness of the structure increases, and the peak deflection at the center of the wall gradually decreases. Since the FE model obtains a high convergence when 30 mm mesh is adopted, considering the accuracy of numerical simulation and computational efficiency under different mesh sizes, the results can be obtained accurately enough with the mesh size of 30 mm. Therefore, throughout the present work, 30 mm × 30 mm × 30 mm solid mesh is used for the block and 30 mm ×30 mm × 10 mm solid mesh for the mortar. The beam element was adopted for the rivet in FE model, and its material model is defined as linear elastic material.

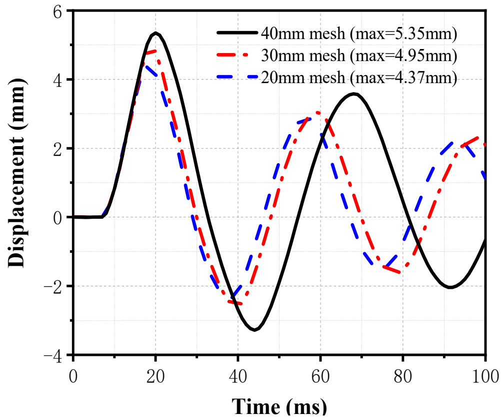

Figure 4. Effect of different mesh size on the simulation results.

In addition, it should be noted that the scope of this study is the non-bearing infilled walls without considering the vertical loading on the wall.

In order to verify the effectiveness of the numerical method to simulate the dynamic response of MIWs under the far-range explosions, seven scenarios of test with relatively complete data carried out by Varma et al. [4] were mainly selected for simulation. The peak reflected overpressure and reflected impulse generated by the blast load on the wall surface measured in each scenario of test, as well as the corresponding peak deflections at the wall center, and the corresponding results obtained by the FE method simulations are presented in Table 3. It can be seen that the simulation results obtained by the FE method show a small deviation compared with the test results, and the deviation of the simulated blast load data is concentrated below 40%, and the deviation of the peak deflection at the wall center is mainly controlled below 20%, while only a relatively large deviation is produced in the simulation of test 3.

Table 3. Test data and numerical simulation results.

<table>
<tr><th colspan="2">Test</th><th>1</th><th>2</th><th>3</th><th>4</th><th>5</th><th>6</th><th>7</th></tr>
<tr><td rowspan="2">Configuration</td><td>Wall thickness (mm)</td><td>230</td><td>230</td><td>340</td><td>460</td><td>340</td><td>340</td><td>460</td></tr>
<tr><td>Boundary</td><td>Plain</td><td>Pin</td><td>Plain</td><td>Plain</td><td>Pin</td><td>Pin</td><td>Pin</td></tr>
<tr><td colspan="2">Charge weight (kg)</td><td>3.3</td><td>21.5</td><td>23.3</td><td>43.2</td><td>50.5</td><td>43.2</td><td>43.2</td></tr>
<tr><td colspan="2">Standoff (m)</td><td>5.0</td><td>4.0</td><td>6.0</td><td>4.25</td><td>3.75</td><td>4.5</td><td>4.25</td></tr>
<tr><td colspan="2">Scaled standoff (m/kg$^{1/3}$)</td><td>3.36</td><td>1.44</td><td>2.10</td><td>1.21</td><td>1.01</td><td>1.28</td><td>1.21</td></tr>
<tr><td rowspan="2">Reflected peak overpressure (MPa)</td><td>Test</td><td>0.126</td><td>1.294</td><td>0.769</td><td>3.311</td><td>5.185</td><td>2.858</td><td>3.311</td></tr>
<tr><td>Simulation</td><td>0.161</td><td>1.516</td><td>0.506</td><td>2.966</td><td>3.867</td><td>2.519</td><td>2.966</td></tr>
<tr><td rowspan="2">Positive durations (ms)</td><td>Test</td><td>3.44</td><td>1.72</td><td>5.15</td><td>N/A</td><td>2</td><td>3.05</td><td>2.32</td></tr>
<tr><td>Simulation</td><td>4.4</td><td>4.8</td><td>5.6</td><td>6.2</td><td>6.6</td><td>6.2</td><td>6.2</td></tr>
<tr><td rowspan="2">Reflected impulse (MPa·ms)</td><td>Test</td><td>0.21</td><td>1.12</td><td>1.213</td><td>2.38</td><td>3.062</td><td>2.232</td><td>2.38</td></tr>
<tr><td>Simulation</td><td>0.206</td><td>1.038</td><td>0.625</td><td>2.047</td><td>2.791</td><td>1.931</td><td>2.047</td></tr>
<tr><td rowspan="2">Peak deflection (mm)</td><td>Test</td><td>5.6</td><td>127.5</td><td>25.5</td><td>30.6</td><td>N/A</td><td>93.8</td><td>31</td></tr>
<tr><td>Simulation</td><td>4.95</td><td>117</td><td>10.8</td><td>30.4</td><td>Collapse</td><td>109</td><td>30.8</td></tr>
<tr><td colspan="2">Damage level</td><td>D</td><td>C</td><td>D</td><td>C</td><td>A</td><td>B</td><td>C</td></tr>
</table>

Figure 5 gives the distribution of the peak blast overpressure along the wall height for different blast distant ranges obtained from the simulation. It can be seen from the figure that the maximum peak overpressure at the wall occurs at the center of the wall along the wall height when the scaled standoff Z is 2.10, which is about 18% higher than the minimum peak overpressure at the wall, but this difference can increase to 32% as the scaled standoff decreases to 1.01. It shows that the overpressure distribution on the wall under the far-range explosion is relatively uniform, and the uniformity of distribution increases with the increase in the scaled standoff.

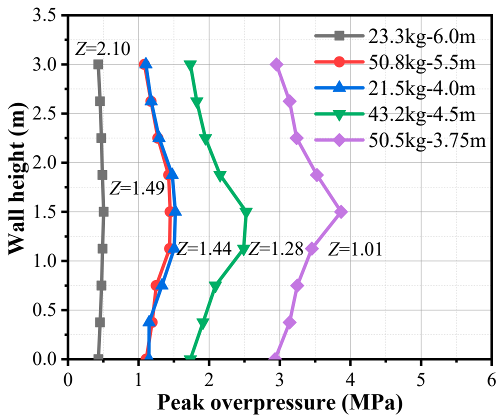

Figure 5. Peak overpressure distribution curve along the wall height.

In summary, under the far-range explosion, because of the relatively uniform distribution of overpressure on the wall, conservative analysis results can be obtained under uniform load with the amplitude of the peak overpressure at the wall center. However, due to the increase in the inhomogeneity of the load distribution as the scaled standoff is further reduced to $Z \leq 1.0\ \mathrm{m/kg^{1/3}}$, the effect of the blast load might be overestimated when the explosion load is simplified to a uniform load with the amplitude of peak overpressure at the wall center.

Varma classified the four damage levels A, B, C, and D according to the final damage results of the wall in the test, from largest to smallest. The final damage patterns of the wall for the four different damage levels obtained from the FE method simulation are given in Figure 6. By comparing with the test data, the simulation obtained a considerably ideal overall damage pattern of the wall. Under the level A damage, the wall shows severe deformation in a large area and produced several large cracks near the four edges of the front surface and the middle of the back, the displacement of the center of the wall was dispersed, and the wall collapsed; under the level B damage, the large deformation was mainly concentrated in the center of the wall and produced main cracks near the four edges and the middle of the back; under the level C damage, the wall deformation is small, and only minor cracks are produced on the wall; Level D damage shows subtle deformation on the wall, and the wall still retains good integrity.

It should be noted that it is still difficult to simulate the localized damage in the class B damage of the wall using the finite element method. Due to the large discrete nature of masonry walls, their local damage is usually related to factors such as the initial damage in the wall and the specific environment of the test, so it is difficult to gain precise simulation results by the FE method. However, the above simulations show that the FE method can provide an effective and accurate simulation of the overall damage pattern and dynamic response of the wall.

Considering the displacement-time histories at the wall center under different damage levels given in Figure 7, it can be seen that: (1) the displacement-time histories at the wall center under the level A damage is diverging, which indicates that the wall has undergone integral damage and no longer has the ability to resist the external load locally, and finally collapses; (2) under the level B damage, although the center displacement of the wall is not diverging to the wall further damaged, large deformation occurs without rebound, which leads to possible local damage to the wall; (3) under level C damage, the wall center displacement is larger, and the occurring of rebound eventually produces relatively large residual deformation; (4) under level D damage, the displacement at the wall center is the smallest, and the wall occurs elastic dynamic response with a certain residual deformation, but much smaller than level C damage.

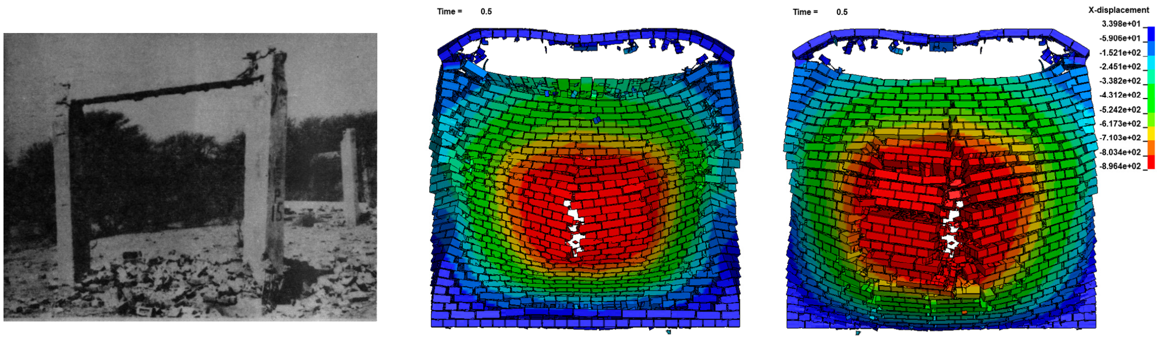

(**a**)

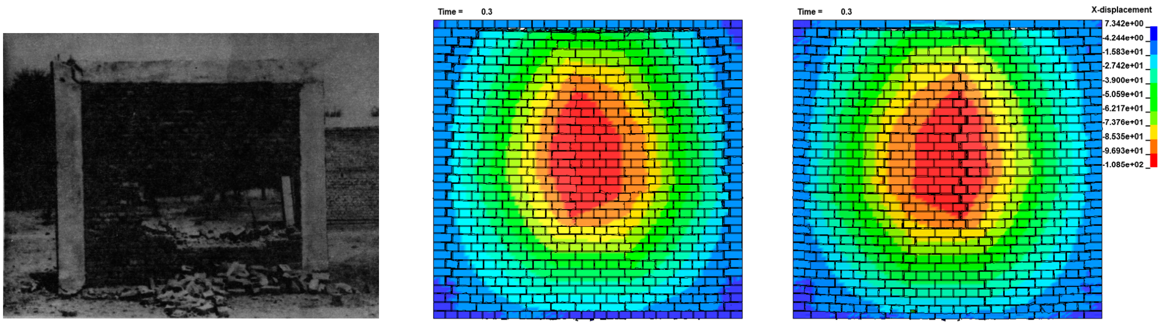

(**b**)

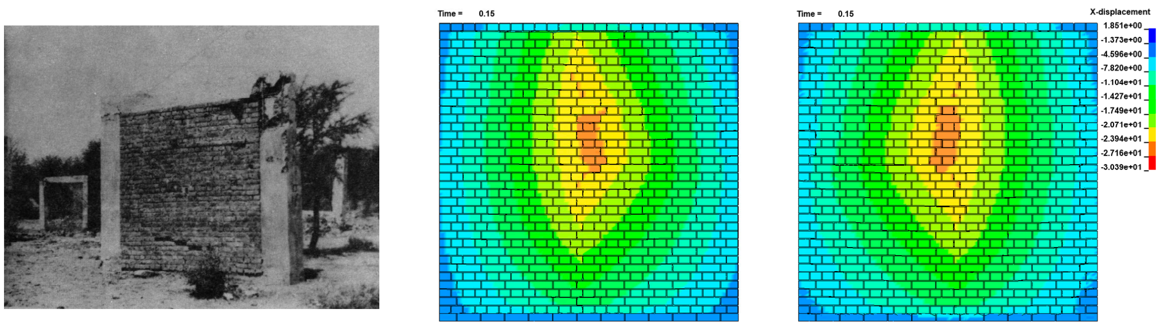

(**c**)

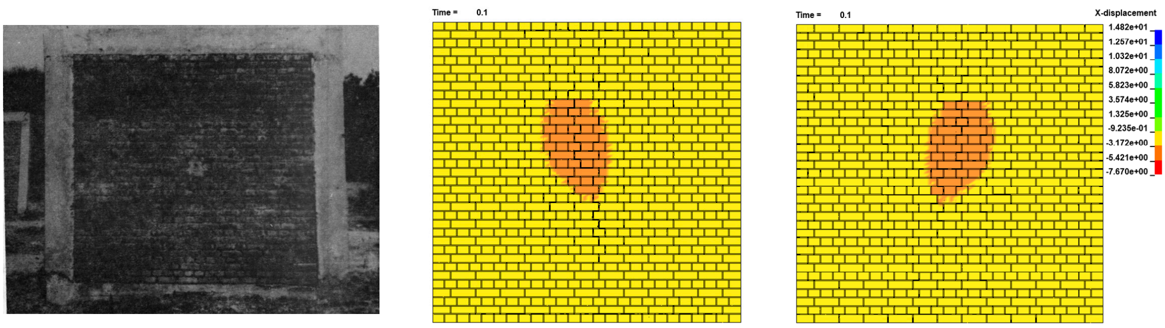

(**d**)

Figure 6. Peak overpressure distribution curve along the wall height: (**a**) Test 5: Level A damage; (**b**) Test 6: Level B damage; (**c**) Test 7: Level C damage; (**d**) Test 3: Level D damage.

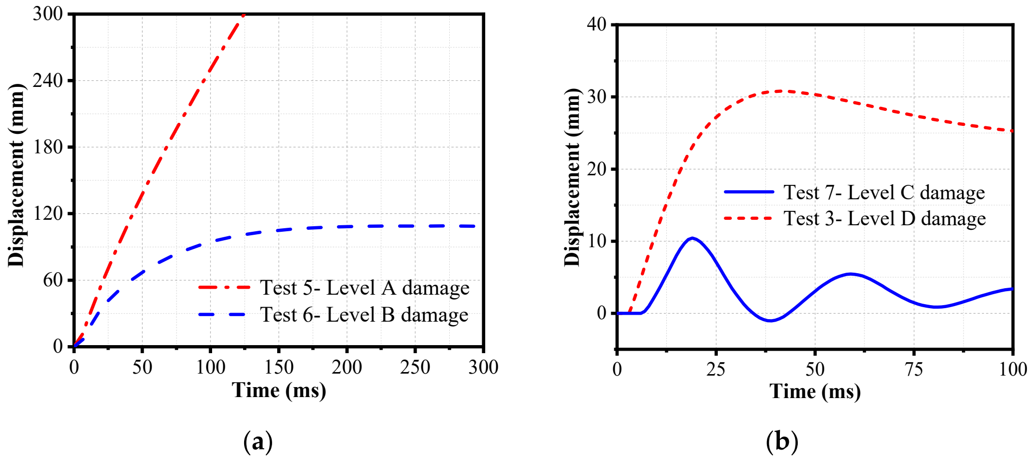

Figure 7. Displacement-time histories at the wall center under different damage levels: (**a**) Level A and B damage; (**b**) Level C and D damage.

In summary, the FE analysis method used in this paper can produce more accurate prediction of the dynamic response of MIW under the far-range explosions, including the displacement-time history and the damage pattern of the wall.

3.2. CMU Masonry Wall Blast Test

For seismic, wind and blast resistance demand, grouted reinforced CMU masonry walls are commonly used in new buildings. Taking into account the needs of practical engineering applications, numerical simulations of two partially grouted CMU MIWs of different thicknesses in the test were carried out in this section, while the validity and accuracy of numerical simulations in analyzing the dynamic response and damage patterns of grouted CMU MIWs were compare and verified. For the blast resistant performance of partially grouted CMU MIWs, Davidson et al. [5] conducted three sets of blast test studies with different scaled standoff. The scaled standoff Z were 3.13 m/kg$^{1/3}$, 2.54 m/kg$^{1/3}$, and 2.03 m/kg$^{1/3}$ for the three tests. Each test consisted of three walls of different configurations, including two grouted CMU MIWs with thicknesses of 6 in. (~150 mm) and 8 in. (~200 mm), and one clay brick veneer double sandwich wall with 2.84m width and 3.45 m height. The construction of the grouted CMU MIW is shown in Figure 8, with the bottom of the wall fixed to a pre-built steel support in the external reinforced concrete frame and the top lapped to the external frame. The 6 in. and 8 in. walls were reinforced with 4 pieces of 9.5 mm diameter and 3 pieces of 12.7 mm diameter steel bars, respectively, and grouted only in the reinforcement masonry holes and the wall end masonry holes. Based on the test setups, the FE model shown in Figure 9 was established.

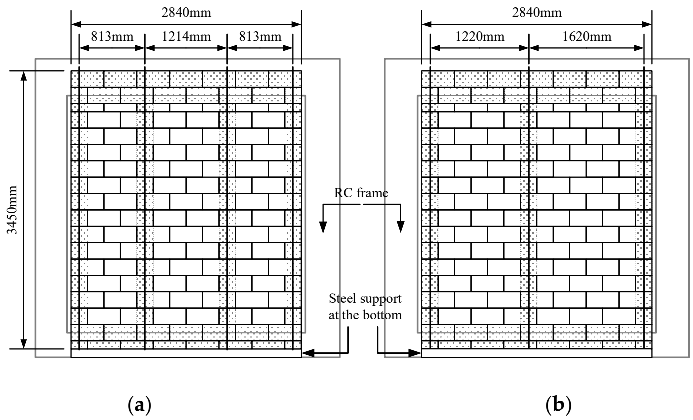

Figure 8. Construction of grouted CMU wall in the test: (**a**) 6 in. wall thickness; (**b**) 8 in. wall thickness.

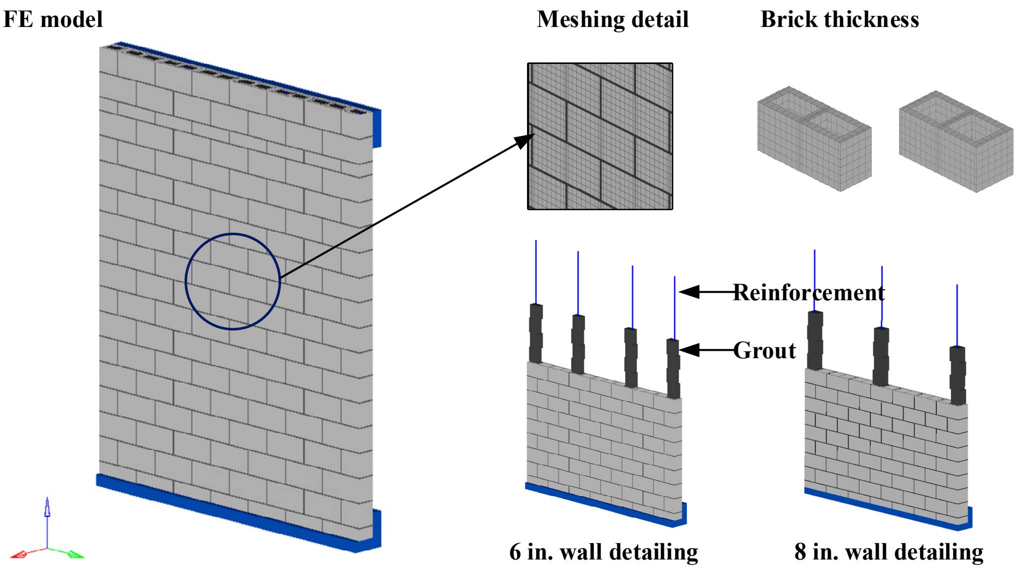

Figure 9. Finite element model of partially grouted CMU MIW.

Additionally, MAT_5 was adopted for blocks in this section, and the values taken for the parameters are listed in Table 2. MAT_3 model is used for reinforcement, and the parameters are listed in Table 4.

Table 4. Steel material model parameters.

Density (kg/m^3)	Young's Modulus (GPa)	Poisson's Ratio	Yield Strength (MPa)	Tangent Modulus (MPa)	Failure Strain
7800	200	0.3	310	400	0.3

Based on the scaled standoff Z, the peak incident overpressure ΔP_s in air can be calculated according to Equation (6) [27].

$$\Delta P_s = \begin{cases} \frac{1.4072}{Z} + \frac{0.554}{Z^2} - \frac{0.0357}{Z^3} + \frac{0.000625}{Z^4} & 0.05 \le Z < 0.3 \\ \frac{0.6194}{Z} - \frac{0.0326}{Z^2} + \frac{0.2132}{Z^3} & 0.3 \le Z < 1 \\ \frac{0.0662}{Z} + \frac{0.405}{Z^2} + \frac{0.3288}{Z^3} & 1 \le Z < 10 \end{cases} \quad (6)$$

The peak reflected overpressure ΔP_{rs} can be calculated from the incident overpressure by the following Equation (7) [28].

$$\Delta P_{rs} = 2\Delta P_s + \frac{6\Delta {P_s}^2}{\Delta P_s + 0.7} \quad \Delta P_s \le 2\text{MPa} \quad (7)$$

According to the above formulas, the peak reflected overpressures in the three blast tests were calculated to be 0.18 MPa, 0.29 MPa and 0.52 MPa, respectively, and the overpressure-time histories are shown in Figure 10.

Figure 11 compares the displacement-time histories curves at the wall center obtained from the simulation and the test. It is easily seen that relatively accurate peak displacements at wall center were obtained using FE simulations for all three tests, with an overall deviation range from 5.8% to 18.9%, for either 6 in. or 8 in. wall thickness grouted CMU MIWs. However, the deflections at the wall center obtained from the simulations were generally smaller than the experimental results, which may be related to the deviation in estimating the peak overpressure of blast loading using the theoretical formulas.

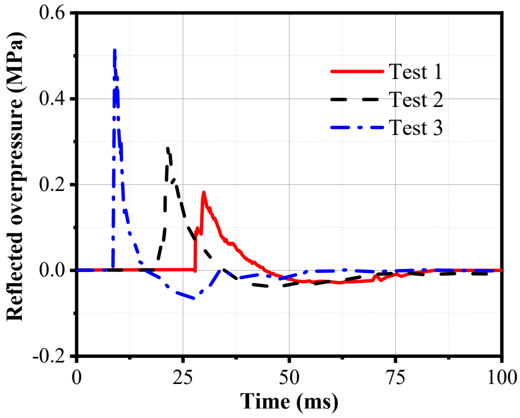

Figure 10. Overpressure-time-histories in the numerical simulations.

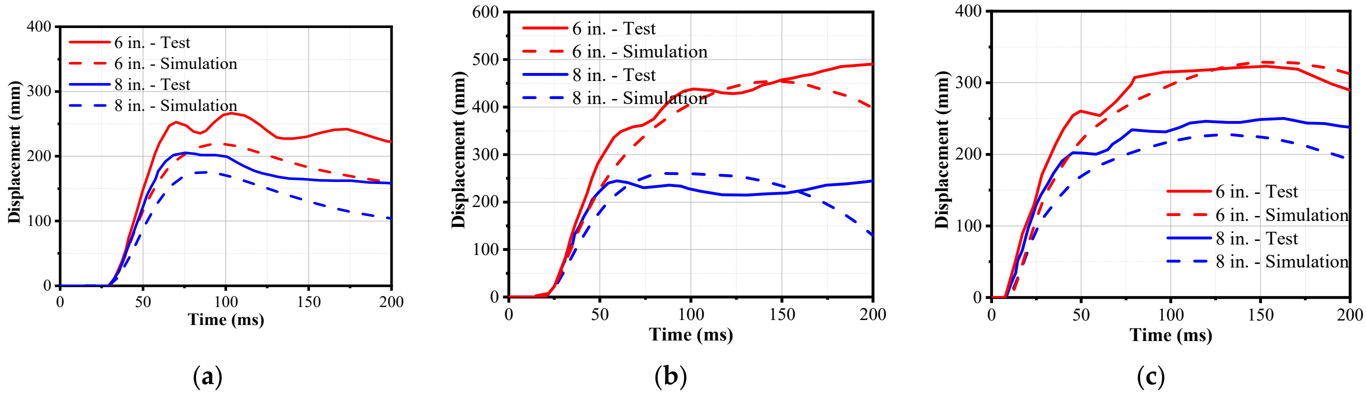

Figure 11. Comparison of displacement-time histories at the wall center: (**a**) Test 1; (**b**) Test 2; (**c**) Test 3.

In general, the shape of the displacement time course curve obtained from the simulations approximates the test data well, but the rebound in the declining phase of the displacement-time history is too large, which indicates that the FE model currently used is still hard to simulate the accumulated damage and residual deformation of the wall after large deformations occur.

Figure 12 further compares the damage pattern of the wall obtained from the simulation at 0.2 s with the final damage pattern of the wall in the test. It can be seen that the overall damage pattern of the wall obtained from the simulation is consistent with the experimental results. Part of the grouted CMU MIW underwent overall unidirectional bending damage and local damage was mainly concentrated at the end and non-grouted block sections. However, for the local damage of the wall, the numerical simulation results deviated from the experimental results to some extent, which was mainly related to the limitation of the simplified load application method in the simulation.

Observing the damage of the walls, it can be seen that under different loading conditions, although the 8 in. wall is thicker and has higher overall reinforcement rate, it went through more severe overall damage because it was less grouted. It can be considered that the grouted ratio of the wall resembles the function of a structural column in the wall, reducing the span in the width and thus slowing down the degree of wall damage. Therefore, in grouted walls, improving the grouting ratio and the uniformity of grout hole distribution can effectively improve the blast resistance of the wall.

In summary, the FE method can effectively predict the dynamic response of partially grouted CMU MIWs under far-range explosions, and predict the peak deformation more accurately, while being able to simulate the overall damage pattern of the wall.

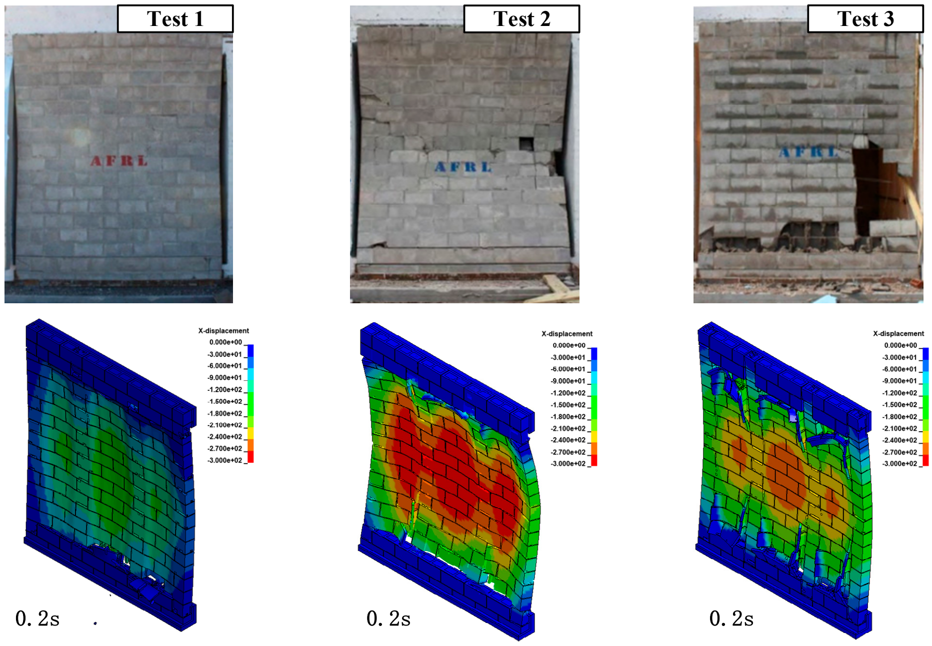

(a)

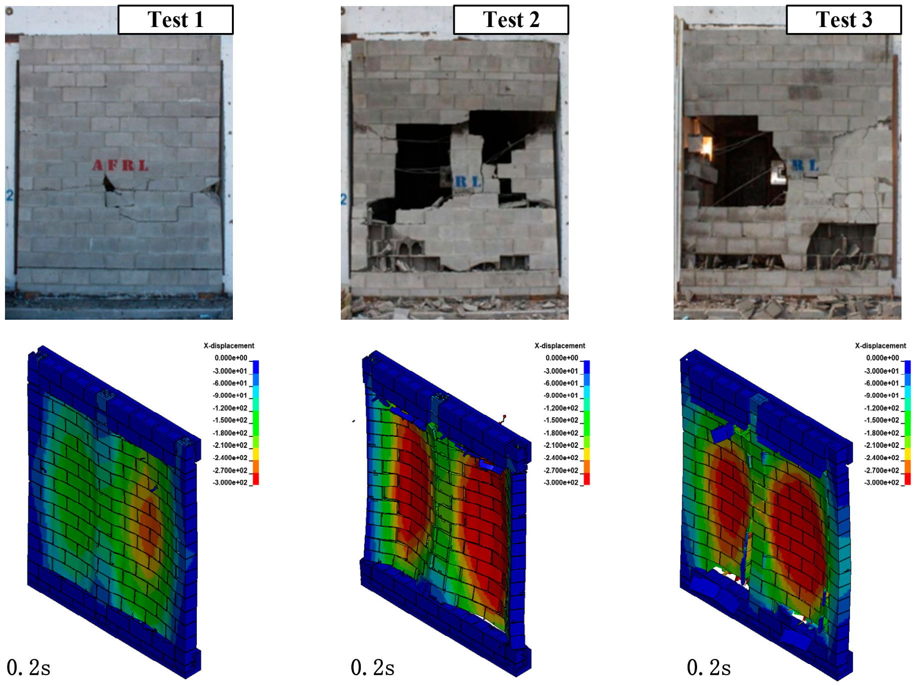

(b)

Figure 12. Comparison of the damage patterns of the walls: (**a**) 6 in. partially grouted CMU wall; (**b**) 8 in. partially grouted CMU wall.

4. Parametric Analysis

This section is mainly based on the clay sintered brick wall model mentioned above, and further develops the parameter sensitivity study for the boundary configuration and constraints of the wall, as well as the wall dimensions to explore the effects of different factors on the dynamic response and damage pattern of the wall under the blast loads.

4.1. Wall Boundary

In this section, based on the FE method, the effects of different wall boundary construction conditions on the dynamic response of the MIW are analyzed under two scenarios: 21.5 kg TNT at 4.0 m standoff ($Z = 1.44$ m/kg$^{1/3}$), and 50.8 kg TNT at 5.5 m standoff ($Z = 1.49$ m/kg$^{1/3}$).

The simulation results of the three different boundary walls under the far-range explosions are shown in Table 5 and Figure 13. It can be seen that there is only a slight difference in the peak displacement at the wall center under different boundary conditions. When the blast load is small and the wall center displacement is not large, the maximum deviation of peak difference is 7.7%. As the blast load increases, the wall center displacement becomes larger, and the maximum deviation is 3.2%. This indicates that under the blast load, since the deformation is usually large, the general wall boundary construction cannot provide effective resistance which has less effect on the dynamic response and damage pattern of the wall.

Table 5. Deflection at the center of walls with different boundary configurations.

Loading	Configuration	Peak Deflection (mm)	Damage Level
Charge weight: 21.5 kg	Plain	124	C
Standoff: 4.0 m	Pin	117	C
Scaled standoff: 1.44 m/kg$^{1/3}$	Groove	126	C
Charge weight: 50.8 kg	Plain	508	A
Standoff: 5.5 m	Pin	504	A
Scaled standoff: 1.49 m/kg$^{1/3}$	Groove	520	A

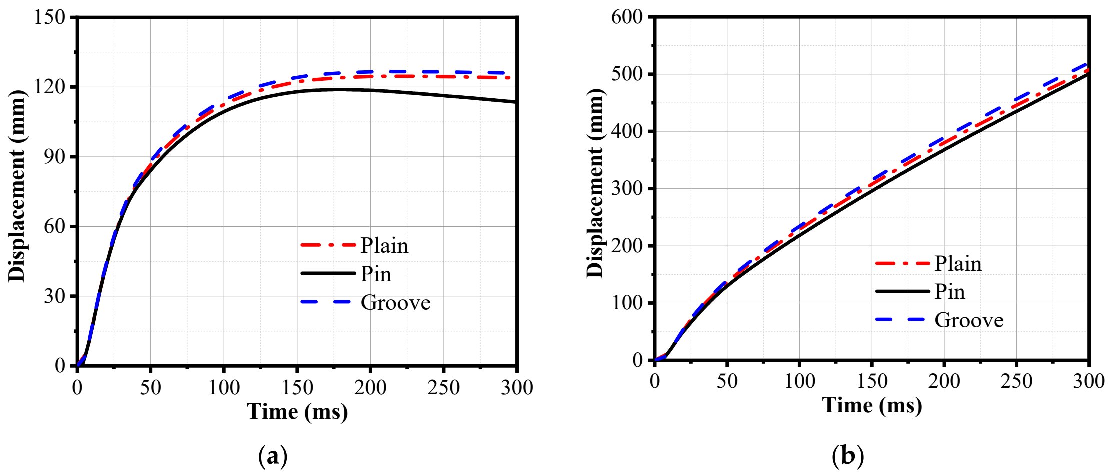

Figure 13. Effect of boundary conditions on the peak displacement at the wall center: (**a**) 21.5 kg–4.0 m–230 mm; (**b**) 50.8 kg–5.5 m–230 mm.

Analyzing the three different boundary configurations, although the effect on the overall dynamic response of the wall and the damage pattern is minor, the pin-type boundary configuration, compared to the other two boundary types, relatively enhances the blast resistance of the wall under different loads due to the presence of structural reinforcement at the boundary. In the case of 21.5 kg charge, it can be found that the structural reinforcement increases the rebound capacity of the wall.

In summary, as the deformation of the wall is usually large under the blast load, the effect of boundary construction form on the dynamic response of the wall is usually weak and no longer plays a significant role.

4.2. Boundary Constraints

This section further explores the effect of different boundary constraints on the blast resistant performance of MIWs. The damage and dynamic response of MIWs with 340 mm are compared and analyzed under blast loads of 23.3 kg TNT charge at 6.0 m standoff ($Z = 2.10\ \mathrm{m/kg^{1/3}}$) and 43.2 kg TNT charge at 4.5 m standoff ($Z = 1.28\ \mathrm{m/kg^{1/3}}$), with one-way, three-side, and four-sided restraints.

Figure 14 shows the final damage pattern of the wall under these three different boundary constraints. It can be seen that with the change of boundary constraints, the damage pattern of the wall changes significantly. With the weakening of the constraint, the large deformation region is mainly shifted to the unconstrained boundary, while the damage region where large deformation occurs increases.

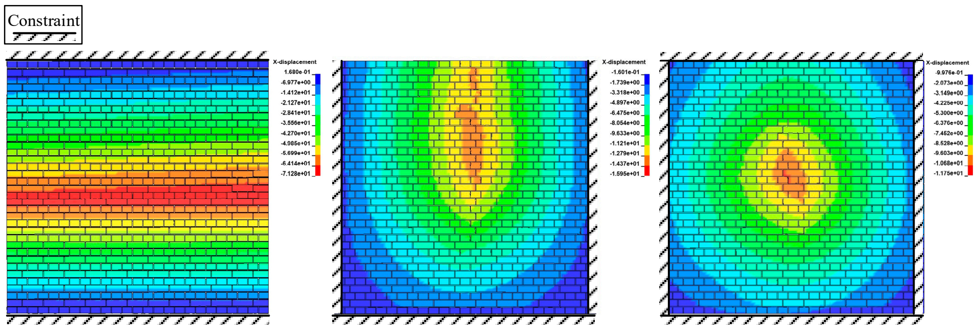

(**a**) (**b**) (**c**)

Figure 14. Comparison of displacement-time histories at the wall center ($Z = 2.10\mathrm{m/kg^{1/3}}$): (**a**) one-way constraint; (**b**) three-side constraint; (**c**) Four-side constraint.

Figure 15 gives the displacement–time histories of the wall center under different constraint conditions. It can be clearly seen that the maximum deflection at the wall center increases rapidly with the weakening of the boundary constraint, and the corresponding damage level of the wall changes. As for the scenarios with $Z = 2.10\ \mathrm{m/kg^{1/3}}$ as an example, the damage of the wall at the four-sided constraint is slight and still retains a high elasticity, which belongs to the level D damage; at the three-sided constraint, it becomes the level C damage and produces a high residual deformation; when the constraint is weakened to the one-way constraint, the damage level of the wall is further aggravated and gradually loses the recovery ability and develops to the level B damage.

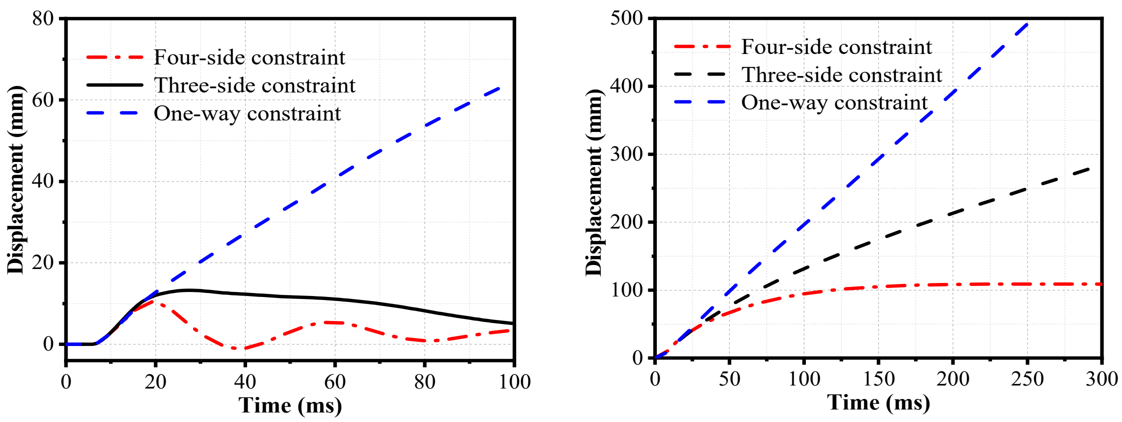

(**a**) (**b**)

Figure 15. Displacement-time histories at the wall center under different boundary constraints: (**a**) 23.3 kg–6 m–340 mm; (**b**) 43.2 kg–4.5 m–340 mm.

4.3. Wall Size

Generally, wall dimensions are an important parameter affecting damage and dynamic response of walls, and in this section, the effects of various wall dimensions on the blast resistant performance of MIWs are further explored based on the FE method. Based on the MIW of 3 m wall height, this section discusses the damage pattern and dynamic response of the wall with 3 dimensions: 2 m wall width (aspect ratio 1.5), 3 m wall width (aspect ratio 1.0), and 4m wall width (aspect ratio 0.75), under blast loading of 50.8 kg TNT charge at standoff of 5.0 m, 21.5kg TNT charge at 4.0 m, and 3.3 kg TNT charge at 5.0 m.

Figure 16 shows the damage pattern of the wall with different wall widths. It can be seen that under the condition of four-sided restraint, the overall damage pattern of the wall under different blast load conditions is similar to that of the four-sided restrained slab, which is mainly stressed along the short side and the main cracks are carried out in accordance with the plastic hinge line theory of the slab. At the same time, with the increase of the overall size of the wall, the final degree of overall damage intensifies.

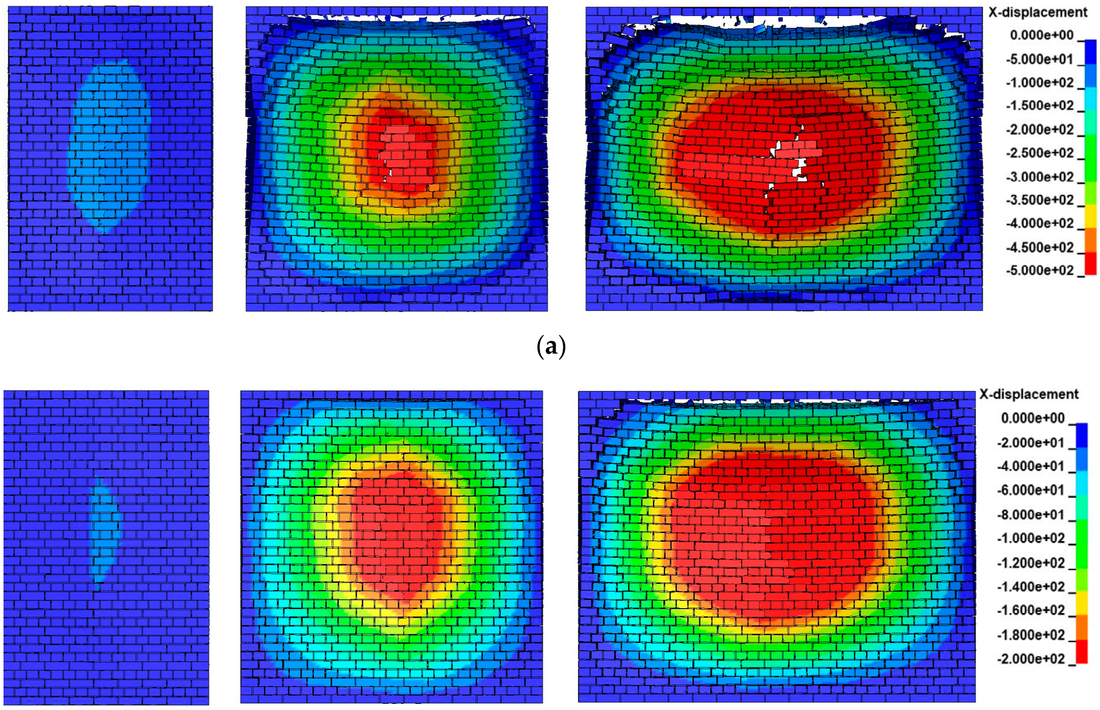

(**a**)

(**b**)

Figure 16. Damage pattern of walls with different widths: (**a**) 50.8 kg charge—5.5 m blast distance—230 mm wall thickness; (**b**) 21.5 kg charge—4.0 m blast distance—230 mm wall thickness.

Figure 17 further gives the displacement-time histories at the wall center under three different blast loads. It can be seen that the damage of the wall is most severe in the case of 4 m × 3 m, while it is least severe in the case of 2 m × 3 m. The reason is that the four-sided constrained boundary conditions, the damage develops mainly along the short side. In the 2 m × 3 m case, the short side is of 2 m, thus the span is reduced, and the final degree of damage is weakened; in the 4 m × 3 m case, although the wall height is still 3 m, but with the increase in width, the wall gradually develops to a 3 m span of the one-way constrained plate, with the weakening of the constraint, the degree of damage intensified.

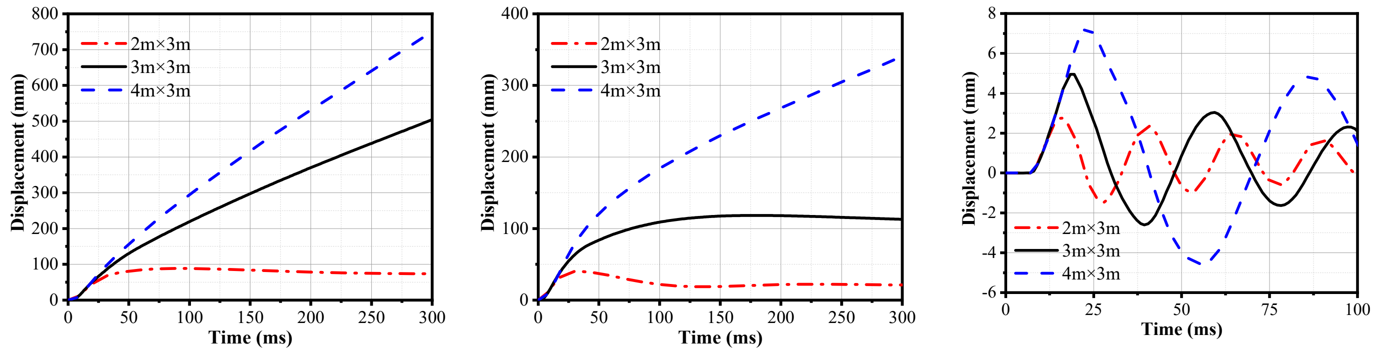

(**a**) (**b**) (**c**)

Figure 17. Effect of wall width on the displacement-time history at wall center: (**a**) 50.8 kg charge—5.5 m blast distance—230 wall thickness; (**b**) 21.5 kg charge—4.0 m blast distance—230 wall thickness; (**c**) 3.3 kg charge—5.0 m blast distance—230 wall thickness.

Figure 18 shows the simulated dynamic response of a 3 m × 3 m MIW of different thicknesses for a 43.2 kg TNT charge at a blast distance of 4.25 m ($Z = 1.21\ \mathrm{m/kg}^{1/3}$).

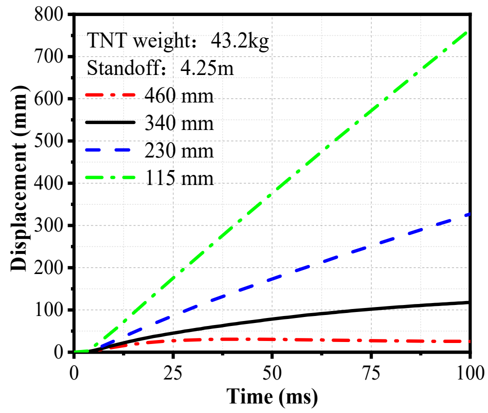

Figure 18. Effect of wall thickness on the displacement at wall center.

It can be seen that the wall thickness is an important influential parameter affecting the damage and dynamic response of MIWs. As the thickness decreases, the maximum displacement at the wall center at the end of the simulation increases exponentially, while the final damage level of the wall varies for different wall thicknesses. For 460 mm wall thickness, the wall occurs more obvious rebound as level C damage; for 340 mm wall thickness, the final displacement of the wall converges as level B damage; for 230 mm and 115 mm wall thickness, the wall collapses completely as level A damage.

5. Conclusions

In this paper, the dynamic response and damage pattern of clay brick MIWs and partially grouted CMU MIWs were simulated under far-range blast loads, mainly based on the tests of Varma [4] and Davison [5], respectively. The accuracy of the FE method was also compared and analyzed by experimental data. In addition, based on the FE model of clay brick MIW, the effects of parameters such as wall boundary configuration, constraints and wall dimensions are further explored. The research results in this paper show that the blast-resistant performance of the wall is significantly related to the boundary connection between the wall and the frame, as well as the thickness of the wall. The blast-resistant performance is significantly improved with the increase of the wall thickness (height thickness ratio) and the enhancement of the frame constraint. Therefore, the constraints of the wall on the four sides to the frame should be considered as priority when constructing the blast-resistant retrofitting of the wall, and the wall thickness shall be increased. The main detailed conclusions are:

(1) The load distribution generated by the far-range explosion on the wall is usually more uniform can be considered by the uniform load. It has been proved that the CONWEP program can effectively simulate the effect of the far-range blast loading.

(2) The grout rate in the grouted wall and uniformity of the grout holes distribution should be enhanced to achieve higher blast resistant performance of the wall.

(3) The influence of boundary configuration is low on the overall response of the wall and damage pattern, with the deviation of deflection less than 15% in the present. Though, strengthening the boundary can increase the integrity and recovery performance of the wall after damage.

(4) The boundary constraints of the wall, length, width, thickness and other dimensional conditions have a significant impact on the response and damage pattern of wall subjected to medium- and far-range explosions. Increasing the wall width can hugely reduce the blast-resistant performance of the wall, while the thickening of the wall has an obvious positive effect on the enhancing of the wall resistance.

Author Contributions: Investigation, Y.Z.; writing—original draft, J.H.; methodology, W.Z.; formal analysis, W.Z.; writing—review and editing, F.H.; validation, X.Y.; visualization, X.Y.; supervision, Y.Z. All authors have read and agreed to the published version of the manuscript.

Funding: This research was funded by National Natural Science Foundation of China grant number 12102476.

Conflicts of Interest: The authors declare no conflict of interest.

References

1. Ettouney, M.; DiMaggio, P.; Hapij, A. Analysis of masonry bearing walls to blast threats. In Proceedings of the Structures Congress, Seattle, WA, USA, 31–29 May 2003.
2. Johnson, C.F. *Concrete Masonry Wall Retrofit Systems for Blast Protection*; Texas A&M University: College Station, TX, USA, 2013.
3. Orton, S.L.; Chiarito, V.P.; Minor, J.K.; Coleman, T.G. Experimental testing of CFRP-strengthened reinforced concrete slab elements loaded by close-in blast. *J. Struct. Eng.* **2014**, *140*, 04013060. [CrossRef]
4. Varma, R.K.; Tomar, C.P.S.; Parkash, S.; Sethi, V.S. Damage to brick masonry panel walls under high explosive detonations. *Asme-Publ. -Pvp* **1996**, *351*, 207–216.
5. Davidson, J.S.; Hoemann, J.M.; Shull, J.S.; Salim, H.A.; Dinan, R.J.; Hammons, M.I.; Bewick, B.T. *Full-Scale Experimental Evaluation of Partially Grouted Minimally Reinforced Concrete Masonry Unit (CMU) Walls Against Blast Demands*; Air Force Research Laboratory (AFRL) Rep. AFRL-RX-TY-TR-2011-0025; Air Force Research Laboratory: Panama, FL, USA, 2011. Available online: https://www.semanticscholar.org/paper/Full-scale-Experimental-Evaluation-of-Partially-Davidson-Hoemann/0e2129c5622c20ed7c27adbaad867add38c68dff (accessed on 14 December 2022).
6. Fang, Q.; Chen, L. Anti-blast properties of masonry infill walls. *Explos. Shock. Waves* **2014**, *34*, 59–66.
7. Keys, R.A.; Clubley, S.K. Experimental analysis of debris distribution of masonry panels subjected to long duration blast loading. *Eng. Struct.* **2017**, *130*, 229–241. [CrossRef]
8. Shi, Y.; Xiong, W.; Li, Z.X.; Xu, Q. Experimental studies on the local damage and fragments of unreinforced masonry walls under close-in explosions. *Int. J. Impact Eng.* **2016**, *90*, 122–131. [CrossRef]
9. Wei, X.; Stewart, M.G. Model validation and parametric study on the blast response of unreinforced brick masonry walls. *Int. J. Impact Eng.* **2010**, *37*, 1150–1159. [CrossRef]
10. Hao, H.; Wu, C. Numerical simulation of damage of low-rise RC frame structures with infilled masonry walls to explosive loads. *Aust. J. Struct. Eng.* **2006**, *7*, 13–22. [CrossRef]
11. Hao, H.; Tarasov, B.G. Experimental study of dynamic material properties of clay brick and mortar at different strain rates. *Aust. J. Struct. Eng.* **2008**, *8*, 117–132. [CrossRef]
12. Michaloudis, G.; Gebbeken, N. Modeling masonry walls under far-field and contact detonations. *Int. J. Impact Eng.* **2019**, *123*, 84–97. [CrossRef]
13. Badshah, E.; Naseer, A.; Ashraf, M.; Ahmad, T. Response of masonry systems against blast loading. *Def. Technol.* **2021**, *17*, 1326–1337. [CrossRef]
14. El-Hashimy, T.; Ezzeldin, M.; Tait, M.; El-Dakhakhni, W. Reinforced masonry shear wall blast response limits for ASCE 59 and CSA S850. *Eng. Struct.* **2021**, *239*, 112183. [CrossRef]
15. Codina, R.; Ambrosini, D. Experimental study of confined masonry walls under blast loading. *Shock. Waves* **2022**, *32*, 261–272. [CrossRef]

16. Chiquito, M.; López, L.M.; Castedo, R.; Pérez-Caldentey, A.; Santos, A.P. Behaviour of retrofitted masonry walls subjected to blast loading: Damage assessment. *Eng. Struct.* **2019**, *201*, 109805. [CrossRef]
17. Shamim, S.; Khan, R.A.; Ahmad, S. Fragility analysis of masonry wall subjected to blast loading. In *Structures*; Elsevier: Amsterdam, The Netherlands, 2022; Volume 39, pp. 1016–1030.
18. Chiquito, M.; Castedo, R.; Santos, A.P.; López, L.M.; Pérez-Caldentey, A. Numerical modelling and experimental validation of the behaviour of brick masonry walls subjected to blast loading. *Int. J. Impact Eng.* **2021**, *148*, 103760. [CrossRef]
19. Li, Z.; Chen, L.; Fang, Q.; Chen, W.; Hao, H.; Zhu, R.; Zheng, K. Experimental and numerical study on CFRP strip strengthened clay brick masonry walls subjected to vented gas explosions. *Int. J. Impact Eng.* **2019**, *129*, 66–79. [CrossRef]
20. Türkmen, Ö.S.; Wijte, S.N.; De Vries, B.T.; Ingham, J.M. Out-of-plane behavior of clay brick masonry walls retrofitted with flexible deep mounted CFRP strips. *Eng. Struct.* **2021**, *228*, 111448. [CrossRef]
21. Mollaei, S.; Babaei Ghazijahani, R.; Noroozinejad Farsangi, E.; Jahani, D. Investigation of Behavior of Masonry Walls Constructed with Autoclaved Aerated Concrete Blocks under Blast Loading. *Appl. Sci.* **2022**, *12*, 8725. [CrossRef]
22. LS-DYNA Keyword User's Manual. *Software*; Technology Corporation (LSTC): Livermore, CA, USA, 2014.
23. CSCEC Northeast Design and Research Institute Co., Ltd. *Code for Design of Masonry Structures*; China Architecture Press: Beijing, China, 2011.
24. Riddington, J.R.; Ghazali, M.Z. Hypothesis for shear failure in masonry joints. *Proc. Inst. Civ. Eng.* **1990**, *89*, 89–102. [CrossRef]
25. Atkinson, R.H.; Amadei, B.P.; Saeb, S.; Sture, S. Response of masonry bed joints in direct shear. *J. Struct. Eng.* **1989**, *115*, 2276–2296. [CrossRef]
26. Davidson, J.S.; Sudame, S.; Dinan, R.J. *Development of Computational Models and Input Sensitivity Study of Polymer Reinforced Concrete Masonry Walls Subjected to Blast*; DTIC Document: Fort Belvoir, VA, USA, 2004.
27. Henrych, J.; Major, R. *The Dynamics of Explosion and Its Use*; Elsevier: Amsterdam, The Netherlands, 1979.
28. Fang, Q.; Liu, J.C. *Underground Protective Structure*; Water and Power Press: Beijing, China, 2010.